J. Fluid Mech. (1969), *vol.* 36, *part* 4, *pp.* 695–720
Printed in Great Britain

The initial ionization of hydrogen in a strong shock wave

By A. N. BELOZEROV† AND R. M. MEASURES
Institute for Aerospace Studies, University of Toronto

(Received 16 July 1968)

A theoretical and experimental investigation has been made of the initial ionization processes in a strong shock wave in hydrogen. The relaxation length for ionization, which is principally determined by the rate of excitation, was measured and from a comparison with the theory an estimate was obtained for the cross-section for atom–atom excitation collisions.

Detailed theoretical calculations showed that the electron temperature approaches to within 1 % of the atomic temperature in a distance that is small compared with the total relaxation length for ionization. This enabled considerable simplification, for it indicated that a single-temperature model could be used in calculating the theoretical relaxation profile over the experimental range of operating conditions. An electromagnetic shock tube, with a Philippov pinch to create the driver plasma, was employed to produce shock waves of the required velocity. The ionization behind the shock front was studied by means of a double-frequency Mach–Zehnder interferometer, with a ruby laser and a K.D.P. crystal as the light source. A close agreement between the theoretical and experimental electron density profiles, behind the shock front, was obtained for small relaxation lengths, when the cross-section for the atom–atom excitation collisions was assumed to be about 7×10^{-2} times that of the corresponding cross-section for electron–atom excitation collisions.

Introduction

The cross-section for ionization by electron impact can be calculated for hydrogen and hydrogen-like types of atoms (Gryzinski 1959; Presnyakov, Sobelman & Vaishtein 1963; Burgess 1963). It can also be obtained by direct experiment using the electron beam technique (Fite & Brackmann 1958; Lichten & Schultz 1959; Stabbings *et al.* 1960). The calculation of the cross-section for the ionization by impact of heavy particles for energies in the range 10–20 eV is considerably more difficult and so far there has been no attempt to solve the problem. The direct experimental so fails owing to the difficulty of obtaining the beam of neutral particles of such energies.

The development of the shock tube technique presented the opportunity for indirect measurements of the above cross-sections for heavy gases. Such a measurement for argon was made recently by Wong & Bershader (1966). Un-

† Present address: Institute of Mechanics, Academy of Science, Moscow, USSR.

fortunately, for light gases, the speed of the shock wave obtained in a conventional type of shock tube is too low to reach the conditions necessary for ionization (Chang 1965). Alternatively, the electromagnetic shock tube is unreliable for such measurements owing to some inborn difficulties such as radiation from the discharge plasma, and the strong interaction of the plasma driver with the shock-heated gas (Ahlstrom *et al.* 1963; McLean & Faneutt 1960; Cloupeau 1963). Some of the above shortcomings inherent in the electromagnetic shock tube were eliminated by Zhurin, Sulyeav & Bukovskii (1963) (see also Zhurin & Sulyear 1963), who used a Philippov pinch (see Philippov, Philippova & Vinogradov 1962 and Philippov & Philippova 1965) as a driver. In the present work the advantages of the above type of electromagnetic shock tube were utilized for the study of the initial ionization processes in a strong shock wave in hydrogen.

Any indirect measurements of cross-sections should be based upon the appropriate theoretical model of the flow behind the shock wave. The basic theory for the ionization behind a shock wave was developed in two papers by Petschek & Byron (1957) and Bond (1957). They showed the importance of the energy equation for the electrons, relating changes in the free electron energy to elastic and inelastic encounters. Weymann (1958) and Harwell & Jahn (1964) showed that the initial ionization rates due to atom–atom collisions involved a two-step process of excitation followed by ionization from the excited state.

Oettinger (1966) has discussed a fairly complete theoretical model in the particular case of argon. He considered radiative as well as collisional processes in the rate and conservation equations. The present theoretical model is very similar to that of Oettinger except that the initial value for the electronic temperature is calculated rather than taken as arbitrary.

It was found that for shock speeds of less than 4 cm/μsec in hydrogen the simple model which assumes that the electronic and atomic temperatures are equal throughout the relaxation region leads to a negligible error in the electron number density profiles behind the shock wave. This is explained by the higher energy transfer rate between the electronic and atomic components of the flow for hydrogen in comparison with argon. This is the consequence of two facts: first the mass of the hydrogen atom is $\frac{1}{40}$ that of the argon atom, and second there is no Ramsauer effect for the electron–hydrogen-atom elastic collisions. The latter effect reduces the cross-section for elastic electron–argon-atom collisions in the energy range of interest.

The experimental electron density profiles behind the shock wave were recorded by a double-frequency interferometric technique. The required time resolution was achieved by using a ruby pulsed laser with a saturable cell giving pulses of about 10 nsec duration. A K.D.P. crystal mounted on the output of ruby laser transformed some of the 6934 Å radiation from the ruby into near-ultraviolet radiation at 3472 Å. By this means almost instantaneous interferograms of the shock wave at two frequencies were recorded.

1. Mathematical formulation

Basic concept of relaxation in strong shocks

A propagating shock wave transforms the initial low-temperature low-pressure gas into the high-temperature high-pressure gas residing behind the shock. In the ideal limit this transformation takes place in an infinitesimal region called the shock front. Since all the changes in the state of a real gas can be achieved by collisions between gas particles, in practice there will be a certain finite distance of approach to the equilibrium state behind the shock front. For moderate shock

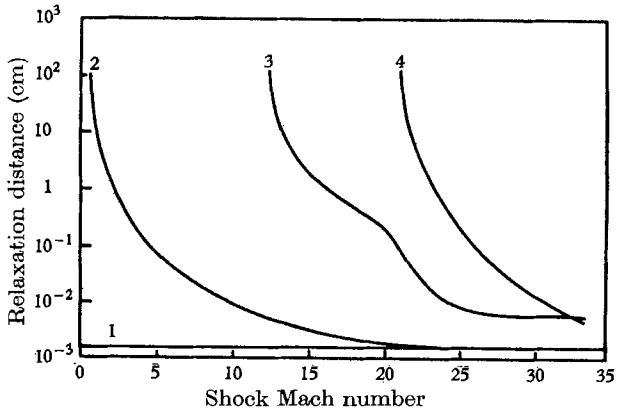

Figure 1. Comparison of relaxation distances behind the shock front in hydrogen. Curves: 1, translation; 2, vibration; 3, dissociation; 4, ionization.

speeds only a few collisions between particles are sufficient to reach an equilibrium since only translational and rotational degrees of freedom of the gas molecules are involved. With increase of the shock speed the kinetic energy of the particles becomes high enough first to excite vibrational degrees of freedom, then to dissociate molecules and finally to ionize the atoms.

The probability, or the cross-section, for the latter processes is much smaller than that required to equilibrate the translational or rotational degrees of freedom so that many collisions are necessary before ionizational equilibrium is reached. Schematically the different relaxation regions and their relative lengths as functions of shock velocity are shown in figure 1. The data in figure 1 were taken from Chang (1962*a*, *b*) for the vibrational and dissociational relaxation lengths respectively, and from the present paper for the ionizational relaxation. A comparison of relaxation lengths shows that for certain intervals of shock velocities it is possible to consider the different relaxation processes independently. For example, ionization can be considered separately from dissociation for shock Mach numbers, $M_s < 27$.

Rate equations for ionization processes

As a result of the previous discussion we can assume that ionization behind the strong shock in hydrogen effectively starts after dissociation is completed. With this assumption there will be no difference between hydrogen and any monatomic gas like argon in the description of the ionization process except for the initial conditions, which in the case of hydrogen will correspond to a fully dissociated gas behind the shock.

Following the established procedure in dealing with multiple and competing processes of excitation, de-excitation, ionization, recombination (see Wong & Bershader 1966; Petschek & Byron 1957; Bond 1957; Oettinger 1966) etc. which lead to the ionizational equilibrium, we separate the whole relaxation region into three subzones each dominated by some principal ionization mechanism. First is the zone of the initial ionization, then the zone where the primary reaction is the ionization by electron impact and last the third zone where recombination becomes important. We now consider each of them in more detail.

The first zone

In this region the most important processes are the atom–atom collisions, photo-ionization and atom–impurity collisions. The atom–atom process may involve two possible mechanisms: (*a*) a single-step ionization

$$\mathrm{H}+\mathrm{H}\rightarrow\mathrm{H}^{+}+\mathrm{e}+\mathrm{H};$$

(*b*) a two-step ionization with an intermediate excited state

$$\mathrm{H}+\mathrm{H}\rightarrow\mathrm{H}^{*}+\mathrm{H},$$

$$\mathrm{H}^{*}+\mathrm{H}\rightarrow\mathrm{H}^{+}+\mathrm{e}+\mathrm{H}.$$

Weymann (1958) showed theoretically that the two-step process is more efficient. His conclusions are based upon the facts that the cross-section (or the probability) for excitation from the ground state is greater than ionization from the ground state and the probability for ionization of an excited state is more favourable than de-excitation.

The microwave study of the initial ionization in noble gases by Harwell & Jahn (1964) showed that the threshold energy corresponds to that of excitation rather than ionization. Since the probability of subsequent ionization of an excited state is several orders of magnitude larger than that for atoms in the ground state, the initial step of the two-step process becomes the rate-controlling one† and we can write the following expression for the rate of electron production by both mechanisms,

$$[dn_e/dt]_a = \tfrac{1}{2}[R_a(1,z)+R_a(1,2)]\,n_a^2. \tag{1.1}$$

The derivation of this formula is given in the appendix.

† Strictly speaking we should consider also excitation into higher excited levels but, as will be shown later during the description of the electron–atom inelastic collisions, their contribution to the reaction is negligible.

In order to relate the above rate coefficients which describe the macroscopic behaviour of the gas with the corresponding microscopic parameters, such as cross-sections, further assumptions about the conditions and the cross-sections themselves have to be made. Since the mean thermal energy of the gas particles is much less than the threshold energy for the range of gas temperatures of interest, a linear approximation near the threshold is assumed,

$$\sigma(E) = A(E - E_0). \tag{1.2}$$

$\sigma(E)$ is the cross-section for excitation to the state having a threshold energy E_0; E is the relative energy of the colliding particles; A is a constant. Assuming a Maxwellian velocity distribution for the colliding particles the rate coefficient for excitation

$$R = A\left(\frac{8}{\pi\mu}\right)^{\frac{1}{2}}(kT)^{\frac{3}{2}}\left(\frac{E_0}{kT}+2\right)\exp\left(-\frac{E_0}{kT}\right), \tag{1.3}$$

where the reduced mass $\mu = \frac{1}{2}m_a$ and k is Boltzmann's constant. In this case we can write

$$\left[\frac{dn_e}{dt}\right]_a = n_a^2\frac{4(kT)^{\frac{3}{2}}}{\sqrt{(\pi m_a)}}\left[A_a(1,z)\left(\frac{E_{\text{ion}}}{kT}+2\right)\exp\left(-\frac{E_{\text{ion}}}{kT}\right)+A_a(1,2)\left(\frac{E^*}{kT}+2\right)\exp\left(-\frac{E^*}{kT}\right)\right], \tag{1.4}$$

where E_{ion} and E^* are the respective energies of ionization and excitation to the first excited state, $A_a(1,z)$ and $A_a(1,2)$ are the approximating linear slopes for the corresponding cross-sections for ionization and excitation.

Of the two forms of radiation that may be thought to be of importance, Lyman-α and Lyman continuum, only the latter is capable of penetrating through to the first zone. However, for the conditions of interest it is insufficient to give a significant contribution to the rate of ionization provided the effective atom–atom cross-section for ionization is greater than about 10^{-3} of the corresponding electron–atom cross-section. The resonance radiation is very strongly absorbed, and it is shown later that this Lyman-α radiation cannot diffuse upstream towards the shock front.

The second and third zones

Eventually the electron number density becomes sufficient for electron–atom collisions to dominate the ionization process. Again, we consider both direct ionization and ionization via an intermediate excited state. The excitation and ionization processes will have their counterparts, corresponding to recombination and de-excitation reactions. The basic processes are consequently ionization and three-body recombination

$$\mathrm{H}(p)+\mathrm{e} \underset{R(z,p)}{\overset{R(p,z)}{\rightleftarrows}} \mathrm{H}^+ + \mathrm{e} + \mathrm{e},$$

collisional excitation and de-excitation

$$\mathrm{H}(p)+\mathrm{e} \underset{R(q,p)}{\overset{R(p,q)}{\rightleftarrows}} \mathrm{H}(q)+\mathrm{e}.$$

We should also consider the following radiative ionization and excitation mechanisms:

photo-ionization and radiative recombination

$$\mathrm{H}(p)+h\nu \underset{\beta(z,p)}{\overset{\beta(p,z)}{\rightleftarrows}} \mathrm{H}^{+}+\mathrm{e};$$

absorption and spontaneous and stimulated emission

$$\mathrm{H}(p) \underset{B(q,p)\rho(\nu)}{\overset{A(p,q) \text{ and } B(p,q)\rho(\nu)}{\rightleftarrows}} \mathrm{H}(q)+h\nu.$$

The rate of change of the number density of excited state p is expressed in terms of the above rate coefficient in the form

$$\begin{aligned} dn(p)/dt = &-n(p)\{n_e[R(p,z)+\sum_{q\neq p} R(p,q)]+\sum_{q<p} A(p,q) \\ &+\rho(\nu_{p,z})\beta(p,z)\}+n_e\sum_{q\neq p} n(q)\,R(q,p)+\sum_{q>p} n(q)\,A(q,p) \\ &+\sum_{q\neq p}\rho(\nu_{q,p})\,n(q)\,B(q,p)+n_e^3 R(z,p)+n_e^2\beta(z,p) \quad (p=1,2\ldots). \end{aligned} \tag{1.5}$$

The collisional–radiative processes which are described by the above system of equations were treated by Bates, Kingston & McWhirter (1962). It follows from the results of their investigation that one can reduce the system of equations (1.5) to only two rate equations for the population of the ground and the first excited state. The population of all but the first excited states are very small,

$$n(p) \ll \{n(1)+n(2)\} \quad (p\neq 1,2)$$

and their quasi-equilibrium value is reached almost instantaneously without the number density of the free electrons being appreciably altered. Thereafter the rates at which excited states are produced and destroyed by collision and radiative processes are much greater than the rates at which the number densities of these states change. That can be mathematically expressed as

$$\sum_{p\neq 1,2}\frac{dn(p)}{dt} \ll \frac{dn(2)}{dt}+\frac{dn(1)}{dt}.$$

The quasi-equilibrium value of the population of the qth state of the atom is related by a modified Saha equation with the electron number density at each particular moment of time

$$n(q) = \frac{n_e^2 h^3}{2(2\pi m_e kT_e)^{\frac{3}{2}}}\frac{g(q)}{g^{+}}\exp\left(\frac{E(q,z)}{kT_e}\right), \tag{1.6}$$

where g^{+} and $g(q)$ are degeneracy factors for the ion and excited atom respectively. The rate of ionization is determined by only two reactions

$$\frac{dn_e}{dt} = -\left[\frac{dn(1)}{dt}+\frac{dn(2)}{dt}\right]. \tag{1.7}$$

Bates *et al.* (1962) showed that for most cases of practical interest the population of the second level also reaches the quasi-equilibrium value in a very short time interval (which is even smaller than the time obtained in the appendix for similar

atom–atom processes). Thus for times of interest the rate of ionization is determined essentially by the rate of depopulation of the ground state

$$\frac{dn_e}{dt} = -\frac{dn(1)}{dt} = [Sn(1) - \alpha n_e]\, n_e, \tag{1.8}$$

where $S = S(T_e, n_e)$ is the collisional–radiative ionization coefficient and $\alpha = \alpha(T_e, n_e)$ is the collisional–radiative recombination coefficient. The values of S and α are tabulated by Bates *et al.* (1962) for different types of plasmas: optically thin, optically thick, in all the lines or in Lyman lines only, etc.

The hydrogen plasma behind the shock wave is optically thick in the Lyman-α line for the conditions prevailing in the present experiment ($T = 10^4$ °K, $n_a = 10^{18}\,\mathrm{cm}^{-3}$, $n_e = 10^{17}\,\mathrm{cm}^{-3}$). The remaining lines are Stark broadened and their optical depths are comparable with the size of plasma behind the shock. Consequently the plasma is considered to be optically thin for all but the Lyman lines. The difference between the rate, $Sn(1)$ and αn_e for this case, and the rate for the case of a fully collision-dominated plasma is shown in figure 2. The difference in the ionization rate coefficient, $Sn(1)$, for the two cases is so small that it cannot be seen on the diagram. The difference in the recombination rate, αn_e, is substantial only for very small electron number densities where the magnitude of the recombination rate coefficient is much smaller than that for the ionization rate. For the electron number densities near the equilibrium where $\alpha n_e \simeq Sn(1)$ the difference in the recombination rate for both plasmas is also small. So we can conclude that the influence of the escaping line radiation in the temperature range from 8×10^3 °K to 16×10^3 °K and for $n_a \simeq 10^{18}\,\mathrm{cm}^{-3}$ is negligible and the hydrogen plasma in the second and third zones can be treated as collision-dominated plasmas.

The results of the analysis by Bates *et al.* are strictly speaking applicable only to uniform plasmas. For a non-uniform case like a flow in the relaxation region behind the shock a further assumption, that the radiative transfer mechanisms are slower than any changes in the state of gas, has to be made. It follows from figure 3 that the resonance radiation can propagate upstream into the flow region behind the shock wave if

$$x_{\mathrm{abs}}/t_{\mathrm{life}} > v_{sh} - v_p, \tag{1.9}$$

where t_{life} is the lifetime of the excited state, $v_{sh} - v_p = u_2$ is the velocity of gas relative to the shock and x_{abs} is the mean absorption length for a photon of the appropriate frequency.

For the Lyman line $x_{\mathrm{abs}} \simeq 10^{-5}$ cm, $t_{\mathrm{life}} \simeq 10^{-9}$ sec and for the typical value of the relative velocity $u_2 = 3 \times 10^5$ cm/sec diffusion of the radiation upstream is not possible because

$$x_{\mathrm{abs}}/t_{\mathrm{life}} \simeq 10^4\,\mathrm{cm/sec},$$

which is smaller than u_2.

Consequently, since in our case radiative transfer is also unimportant the ionization rate will, in zones 2 and 3, be determined only by collisional processes and instead of the system of equations (1.5) the following rate equations can be used:

$$[dn_e/dt]_e = [R_e(1, z) + R_e(1, 2)]\, n_e n_a - R_e(z, 1)\, n_e^3. \tag{1.10}$$

The rate coefficients $R(1,z)$ and $R(1,2)$ can be related to the appropriate cross-sections $A_e(1,z)$ and $A_e(1,2)$ by (1.3). The recombination rate coefficient $R_e(z,1)$ can be expressed in terms of $R_e(1,z)$ by the principle of detailed balance

$$R_e(z,1) = R_e(1,z)/K(T_e),$$

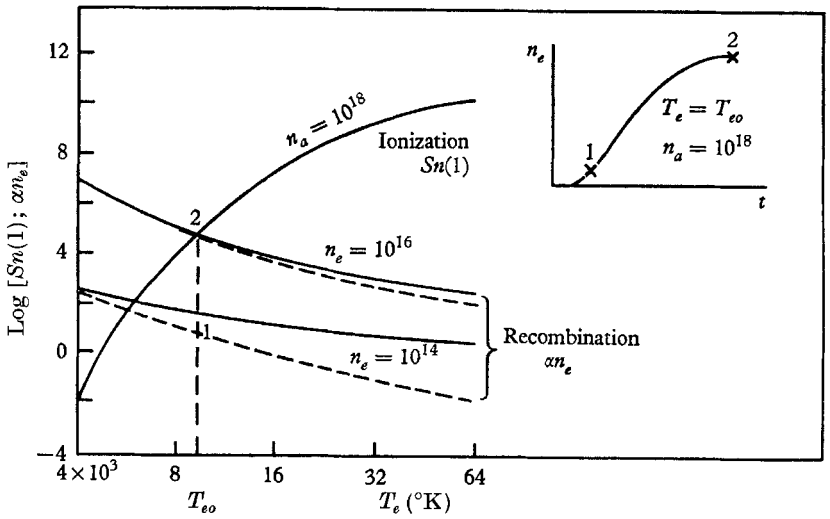

Figure 2. Theoretical ionization and recombination rate coefficient for two types of plasma (Bates *et al.* 1962). ——, plasma optically thick for L-lines; – – –, plasma collisionally dominated.

where the equilibrium constant $K(T_e)$ can be written in the form

$$K(T_e) = \frac{g^+}{g(1)} \frac{(2\pi m_e kT_e)^{\frac{3}{2}}}{h^3} \exp\left(-\frac{E_{\text{ion}}}{kT_e}\right). \tag{1.11}$$

Upon the substitution of the expressions (1.3) and (1.11) into (1.10)

$$\left[\frac{dn_e}{dt}\right]_e = n_a n_e \frac{2\sqrt{2}(kT_e)^{\frac{3}{2}}}{\sqrt{(\pi m_e)}} \left[A_e(1,z)\left(\frac{E_{\text{ion}}}{kT_e}+2\right)\exp\left(-\frac{E_{\text{ion}}}{kT_e}\right) + A_e(1,2)\left(\frac{E^*}{kT_e}+2\right)\exp\left(-\frac{E^*}{kT_e}\right)\right] - \left\{A_e(1,z)\, 2h^3\left[\frac{E_{\text{ion}}}{kT_e}+2\right]\Big/\pi^2 m_e^2\right\} n_e^3. \tag{1.12}$$

Fite & Brackmann (1958) experimentally measured the cross-section for the $(1s,2p)$ and $(1s,z)$ transitions; Lichten & Schultz (1959) and Stabbings *et al.* (1960) obtained the experimental value for the forbidden $(1s,2s)$ transition. Figure 4 shows the values of the cross-sections for the $(1s,2p)$ and $(1s,2s)$ transitions from the above references, together with the linear approximation which was used in the present calculation

$$\sigma_e(1s,2p) + \sigma_e(1s,2s) = A_e(1,2)\,(E^* - E) = 5{\cdot}1 \times 10^{-17}(10{\cdot}2 - E)\,[\text{cm}^2], \tag{1.13}$$

where E is in eV.

For the cross-section of the $(1s,z)$ transition we used the following approximation:

$$\sigma_e(1s,z) = A_e(1,z)\,(E_{\text{ion}} - E) = 5{\cdot}9 \times 10^{-18}(13{\cdot}53 - E)\,[\text{cm}^2]. \tag{1.14}$$

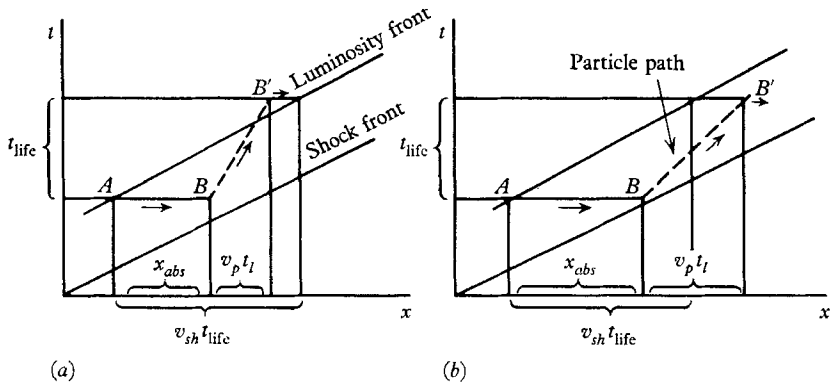

FIGURE 3. Schematic diagram of radiation diffusion.
(*a*) Diffusion is not possible. (*b*) Diffusion is possible.

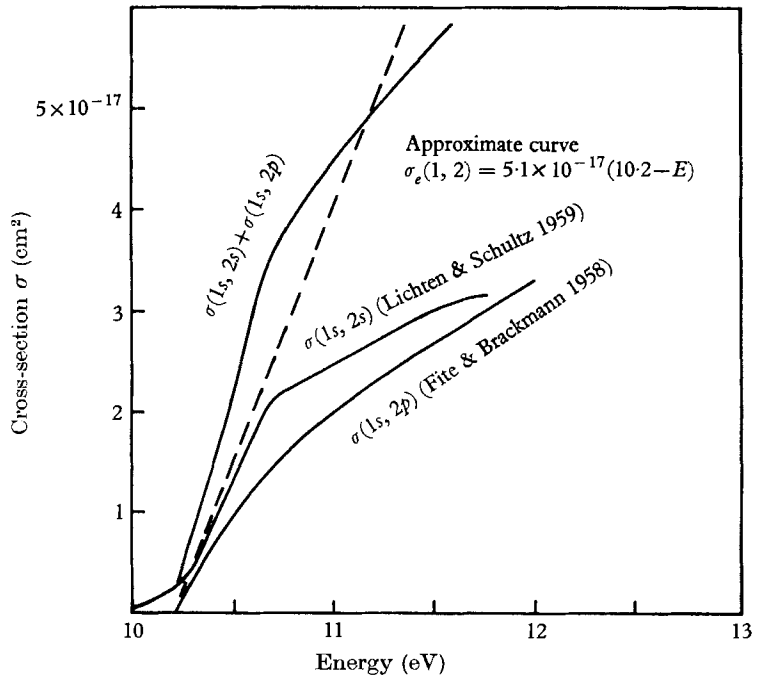

FIGURE 4. Cross-section of the excitation of atomic hydrogen by electron impact.

Equations (1.12) and (1.4) give the rate of ionization in the hydrogen gas as a function of four parameters: electronic and atomic number densities n_e, n_a and the temperature of the electrons and atoms T_e, T_a. The laws of conservation applied to the flow through the shock front and the energy balance between the electronic and atomic components of the flow supply the additional relations between n_e, n_a, T_e, T_a.

Conservation equations

Conservation equations for the gas flow behind the strong non-attenuating shock wave can be written in the co-ordinate system moving with the shock in the following form:

(*a*) mass $$m_a n_{a0} u_0 = m_a(n_a+n_i)\,u; \tag{1.15}$$

(*b*) momentum $$p_0+n_{a0}m_a u_0^2 = p+(n_i+n_a)\,m_a u^2; \tag{1.16}$$

(*c*) energy $$E_0+\frac{p_0}{n_{a0}m_a}+\frac{u_0^2}{2} = E+\frac{p}{(n_a+n_i)\,m_a}+\frac{u^2}{2}; \tag{1.17}$$

where index 0 refers to the state of gas behind the dissociative shock.

Using the two-temperature equation of state in the form

$$p = (n_a+n_i)\,k(T_a+\alpha T_e) \tag{1.18}$$

and the expression for the specific internal energy of the partially ionized gas in the form

$$E = \frac{3}{2}\frac{k}{m_a}(T_a+\alpha T_e)+\frac{\alpha E_{\text{ion}}}{m_a}, \tag{1.19}$$

where $\alpha \equiv n_e/(n_a+n_i)$ is degree of ionization, we obtain after some algebraic manipulations the following two equations relating n_a, α, T_a and T_e:

$$\bar{n} = \frac{1+c+\sqrt{\{\frac{9}{25}c^2-(\frac{6}{5}-\frac{32}{25}\alpha\theta_{\text{ion}})c\}}}{2-\frac{4}{5}\alpha\theta_{\text{ion}}+\frac{2}{5}c}, \tag{1.20}$$

$$\theta_a+\alpha\theta_e = (1/\bar{n}^2)\,[\bar{n}+(\bar{n}-1)\,c], \tag{1.21}$$

where we introduce the dimensionless parameters

$$\theta_a = T_a/T_0, \quad \theta_e = T_e/T_0, \quad \bar{n} = (n_a+n_i)/n_{a0}$$

and

$$\theta_{\text{ion}} = E_{\text{ion}}/kT_0, \quad c = m_a u_0^2/kT_0.$$

The above conservation equations apply to the whole flow and do not provide us with the information concerning the distribution of energies between components of this flow, atoms and electrons. The energy equation for the electronic component is considered next.

Electron energy equation

The competing processes of energy losses in inelastic encounters with atoms and energy gain in elastic collisions with atoms and ions determine the law governing the change of electron energy. With the assumption that there is no diffusion of electrons with respect to ions and atoms and neglecting Bremsstrahlung

radiation losses the rate of change of electron energy in unit time is expressed in the form† $$\frac{d(\frac{3}{2}kT_e n_e)}{dt} = \Delta E_{\text{init}}\left[\frac{dn_e}{dt}\right]_a + Q_{ae} n_a n_e + Q_{ei} n_e^2 - E_{\text{ion}}\left[\frac{dn_e}{dt}\right]_e. \tag{1.22}$$

We consider each term on the right-hand side of the equation separately.

Energy gain in atom–atom collisions

This term describes the energy which electrons possess when they are produced in atom–atom ionizing collisions and determines the initial conditions for the electronic temperature. In order to calculate ΔE_{init} we should know the energy distribution between three particles, atom, ion and electron, resulting from each of the atom–atom ionizing encounters. Unfortunately, there are no theoretical or experimental data available with regard to this aspect of the collision. The most logical assumption that can be made in this case is the assumption of equipartition of energy between the resulting particles.

If the energy of the relative motion of the two atoms before a collision was $\frac{1}{2}\mu g^2$ the resulting energy of each electron under the above assumption would be

$$\epsilon_e = \tfrac{1}{3}[\tfrac{1}{2}\mu g^2 - E_{\text{ion}}].$$

The energy received by all the electrons per cm^3 per sec as a result of ionization by atom–atom collisions is

$$n_a^2 \int_{g_0}^{\infty} \sigma_a(g)\, \epsilon_e(g)\, gf(g)\, dg$$

and the average energy per electron is

$$\Delta E_{\text{init}} = \int_{g_0}^{\infty} \sigma_a(g)\, \epsilon_e(g)\, gf(g)\, dg \Big/ \int_{g_0}^{\infty} \sigma_a(g)\, gf(g)\, dg. \tag{1.23}$$

Assuming as always a Maxwellian distribution and approximating the cross-section in the adopted manner the expression (1.23) can be integrated, which results in the following formula for the initial electron energy:

$$\Delta E_{\text{init}} = \tfrac{2}{3}kT_a \frac{E_{\text{ion}} + 3kT_a}{E_{\text{ion}} + 2kT_a}. \tag{1.24}$$

A more accurate expression can be readily obtained if we consider also the ionization from the first excited level; in which case the final form of the initial electron energy where both direct ionization and ionization from the first excited state are taken into account is

$$\Delta E_{\text{init}} = \tfrac{2}{3}kT_a \frac{E^*_{\text{ion}} + 3kT_a}{E^*_{\text{ion}} + 2kT_a}\left\{1 - \frac{1}{2}\frac{A_a(1,z)}{A_a(1,2)} \times \frac{(E_{\text{ion}} - E^*_{\text{ion}})\, kT_a}{(E^*_{\text{ion}} + 3kT_a)[(E^* + 2kT_a)\exp(E^*_{\text{ion}}/kT_a) + \frac{1}{2}(E_{\text{ion}} + 2kT_a)]}\right\}, \tag{1.25}$$

where $E^*_{\text{ion}} = E_{\text{ion}} - E^*$ is the ionization potential of the first excited level.

† It is necessary to mention that the requirement of a Maxwellian distribution for the electron velocities has to be maintained at each moment, which is not obvious when there is a continuous drain of highly energetic electrons for ionization. A certain time is required to fill the tail of the Maxwellian distribution. Fortunately, as is shown in deBoer (1967), the time required to populate the high-energy tail in the distribution is small in comparison with the relaxation time for ionization.

Energy transfer in elastic electron–atom encounters

The rate of energy transferred to the electrons by atoms during the elastic collisions was computed by Petschek & Byron (1957),

$$Q_{ae} = \frac{m_e^2(T_a - T_e)}{m_a T_e} \int_0^\infty g^3 \sigma_{el}(g) f_e(g)\, dg, \tag{1.26}$$

where $\sigma_{el}(g)$ is the cross-section of the elastic collisions. The experimental data (see Glass & Hall 1959), theoretical curve (see Wiese, Berg & Griem 1960) and approximating curve

$$(\sigma_{el})_{\text{app}} = \begin{cases} \sigma_R \left[1 - \dfrac{E}{E_R}\right] & (E \leqslant E_R), \\ 0 & (E > E_R), \end{cases} \tag{1.27}$$

are plotted in figure 5.

The values of σ_R and E_R were taken to be $\sigma_R = 1{\cdot}78 \times 10^{-15}\,\text{cm}^2$ and $E_R = 14\,\text{eV}$.

Upon substituting for $(\sigma_{el})_{\text{app}}$ the expression (1.26) becomes

$$Q_{ae} = \frac{4\sigma_R}{\sqrt{\pi}} \left(\frac{m_e^2}{m_a}\right) \left(\frac{2kT_e}{m_e}\right)^{\frac{3}{2}} \left(\frac{T_a}{T_e} - 1\right) \left[1 - 3\frac{T_R}{T_e} + \exp\left(-\frac{T_R}{T_e}\right) \left(\frac{T_R}{2T_e} + 2 + 3\frac{T_e}{T_R}\right)\right],$$

where $$T_R = E_R/k.$$

The last term in the square brackets can be omitted in calculations as being much smaller than unity.

Energy transfer in elastic electron–ion encounters

The energy transfer from ions to electrons is determined by the Coulomb cross-section. The resulting equation for energy gain in these collisions is

$$Q_{ei} = \frac{e^4}{m_a} \left(\frac{8\pi m_e}{kT_e}\right)^{\frac{1}{2}} \left(\frac{T_a}{T_e} - 1\right) \ln \Lambda, \tag{1.28}$$

where $$\Lambda = \frac{9(kT_e)^3}{4\pi n_e e^6}.$$

Now we have all the necessary information for the equation (1.22) which completes the system of equations (1.12), (1.4), (1.20) and (1.21) for the ionizational relaxation behind the strong shock in hydrogen.

Initial conditions

In the case of no precursor effects the initial conditions for the ionization relaxation would correspond to the parameters of the gas behind the shock wave with complete dissociation providing that the shock is strong enough. The Rankine–Hugoniot relation for a dissociating gas can be written in the form (Wetzel 1964)

$$\left.\begin{aligned} \rho_0/\rho_\infty &= 2\beta - 1, \\ p_0/p_\infty &= 2\gamma_1 M_s^2(\beta - 1)/(2\beta - 1), \\ T_0/T_\infty &= 2\gamma_1 M_s^2(\beta - 1)/2(2\beta - 1)^2, \\ \beta &= \frac{7 + 3\alpha_d}{2(1 + \alpha_d)} + \frac{E_{\text{vib}}}{kT_0} \frac{1 - \alpha_d}{1 + \alpha_d} + \frac{\alpha_d}{1 + \alpha_d} \frac{E_{\text{dis}}}{kT_0}, \end{aligned}\right\} \tag{1.29}$$

where index ∞ refers to conditions ahead of the shock.

For the strong shocks with the degree of dissociation $\alpha_d \simeq 1$ the equation for β becomes

$$\beta = \tfrac{5}{2} + (E_{\rm dis}/2kT_0)$$

and system (1.29) can be rewritten in the form

$$\left.\begin{aligned} \beta &= \frac{3{\cdot}5\bar{M}_s^2 - 4 + \sqrt{[(2{\cdot}25\bar{M}_s^2 + 16)\,\bar{M}_s^2]}}{2(\bar{M}_s^2 - 4)}, \\ \rho_0/\rho_\infty &= n_{a0}/n_{a\infty} = 2\beta - 1, \\ T_0 &= E_{\rm dis}/k(\beta - 2{\cdot}5), \end{aligned}\right\} \tag{1.30}$$

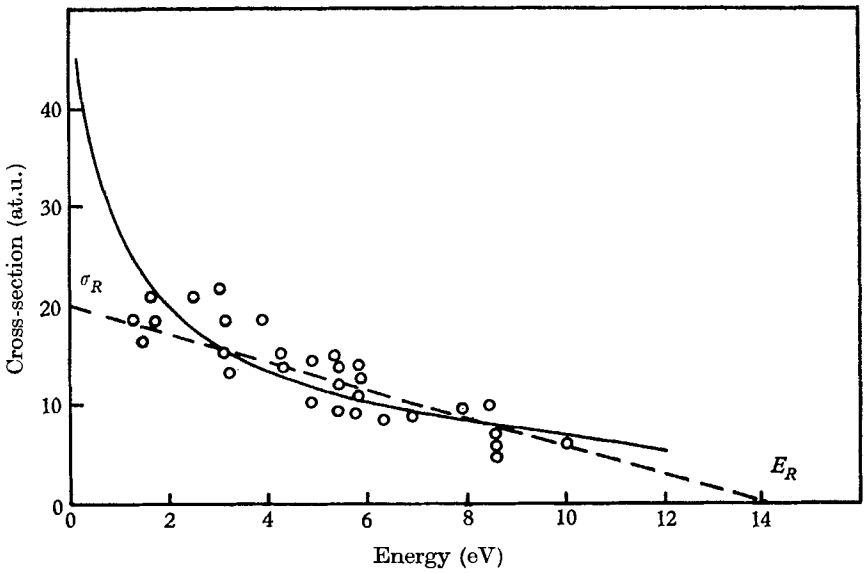

FIGURE 5. Cross-section for the electron–hydrogen-atom elastic collisions (1 at. u. $\equiv \pi a_0^2$, where a_0 is the first Bohr radius). O, experiment, Glass & Hall (1959); ———, theory, Wiese *et al.* (1960); – – –, approximate curve.

where

$$\bar{M}_s = M_s \sqrt{\left[\frac{2\gamma_1 kT_\infty}{E_{\rm dis}}\right]}.$$

The solution of this system of equations for the range of shock speeds of interest is given in figure 6.

The initial value of the electron temperature can be calculated from (1.25). The problem of evaluating the initial electron number density is more complex, for many workers (McLean & Faneutt 1960; Wiese *et al.* 1960; Wetzel 1964; Appleton 1966) have shown that free electrons can exist ahead of the shock front. The source for these precursor electrons in most cases was believed to be the radiation from either the shock-heated gas or the discharge, in electromagnetic shock tubes. A simple microwave transmission experiment was used in the present work to show that the free electron density ahead of the shock was below $10^{13}\,{\rm cm}^{-3}$, which corresponds to a degree of ionization of less than 10^{-5}.

As for preheating of the gas ahead of the shock, the existence of which was

strongly argued by Wiese *et al.* and McLean & Faneutt, we have only indirect evidence that in the present experiments this effect was of no importance. First of all, their experiments where they found the preheating were conducted in T-tubes at a distance of several cm from the discharge the radiation from which is believed to be the source of the preheating. The distance between the observation point and discharge chamber in the present shock tube is about 10 times

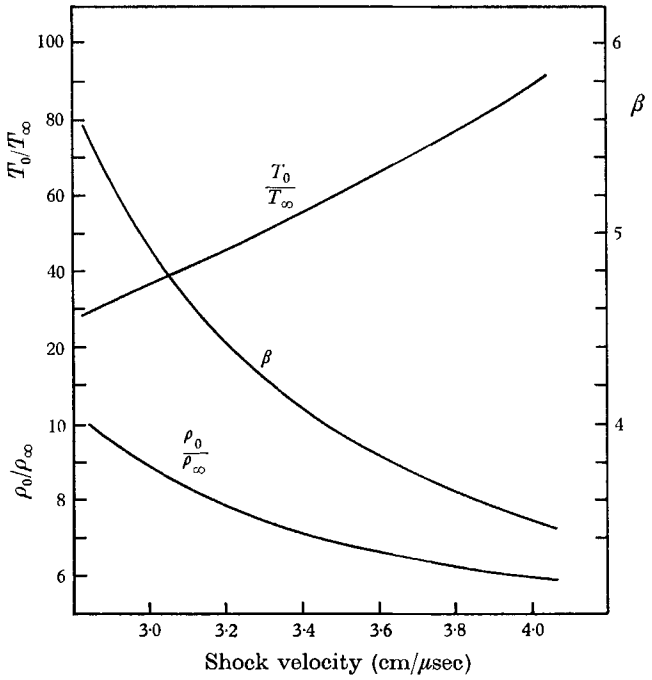

FIGURE 6. State of hydrogen behind the dissociative shock wave.

longer (65 cm) so that one would expect that the ultraviolet radiation would be considerably weakened before it reaches the observation point. Secondly, as a result of the preheating Wiese *et al.* found a strong disparity between the experimentally measured conditions behind the shock and those predicted from the Rankine–Hugoniot relations. In the present experiment the value of the free electron density in the equilibrium region is in reasonable agreement with that predicted.

As a result of the above discussion we conclude that the precursor effects are small and initial conditions for n_a, n_e, T_a are determined by the state of gas behind the dissociative shock and an initial electron number density of not more than $10^{13}\,\mathrm{cm}^{-3}$. Calculations of the relaxation length performed for different n_{e0} in the interval from 0 to $10^{13}\,\mathrm{cm}^{-3}$ did not show any noticeable changes in the results for the range of interest.

For the convenience of making a comparison between the theory and the experiment we consider the growth of ionization in the frame of reference moving with the shock. If steady conditions prevail and the velocity of the species

relative to the shock front u is constant then we may replace the total time derivative by the corresponding spatial part of the convective derivative:

$$\frac{d(n_e, T)}{dt} = u\frac{d(n_e, T)}{dx}, \tag{1.31}$$

where x is the distance from the shock front to any point in the relaxation region at a given moment of time.

The system of equations (1.12), (1.4), (1.20), (1.21), (1.22) can be written in the following final form:

$$\begin{aligned}
d\alpha/d\bar{x} &= s_{aa}(1-\alpha)^2 + s_{ae}\alpha(1-\alpha) - s_{eei}\alpha^3,\\
d\theta_e/d\bar{x} &= (2/3\alpha)\,[q_{aa}(1-\alpha)^2 + q_{ae}\alpha(1-\alpha) + q_{ie}\alpha^3 - (\tfrac{3}{2}\theta_e + \theta_{\text{ion}})\,d\alpha/d\bar{x}],\\
\theta_a + \alpha\theta_e &= (1/\bar{n}^2)\,[\bar{n} + (\bar{n}-1)\,c],\\
\bar{n} &= \frac{1 + c + \{\frac{9}{25}c^2 - (\frac{6}{5} - \frac{32}{25}\alpha\theta_{\text{ion}})\,c\}^{\frac{1}{2}}}{2 - \frac{4}{5}\alpha\theta_{\text{ion}} + \frac{2}{5}c},
\end{aligned} \tag{1.32}$$

where the source functions s and q are

$$s_{aa} = \tfrac{1}{2}\bar{A}_a(1,2)\left\{\frac{2m_e}{m_a}\right\}^{\frac{1}{2}}\bar{n}^2\sqrt{\theta_a}\,\frac{\theta^* + 2\theta_a}{\theta^* + 2}\exp\left(\theta^* - \frac{\theta^*}{\theta_a}\right)$$
$$\times\left[1 + \frac{A_a(1,z)}{A_a(1,2)}\,\frac{\theta_{\text{ion}} + 2\theta_a}{\theta^* + 2\theta_a}\exp\left(-\frac{\theta^*_{\text{ion}}}{\theta_a}\right)\right],$$

$$s_{ae} = \bar{n}^2\sqrt{\theta}\,\frac{\theta^* + 2\theta_e}{\theta^* + 2}\exp\left(\theta^* - \frac{\theta^*}{\theta_e}\right)\left[1 + \frac{A_e(1,z)}{A_e(1,2)}\,\frac{\theta_{\text{ion}} + 2\theta_e}{\theta^* + 2\theta_e}\exp\left(-\frac{\theta^*_{\text{ion}}}{\theta_e}\right)\right],$$

$$s_{eei} = \frac{h^3 n_{a0} e^{\theta^*}}{(\pi m_e k T_0)^{\frac{3}{2}}}\,\frac{A_e(1,z)}{A_e(1,2)}\,\bar{n}^3\,\frac{(\theta_{\text{ion}} + 2\theta_e)}{(\theta^* + 2)\,\theta_e},$$

$$q_{aa} = \left\{\frac{2}{3}\theta_a\,\frac{\theta^*_{\text{ion}} + 3\theta_a}{\theta^*_{\text{ion}} + 2\theta_a}\left[1 - \frac{1}{2}\,\frac{A_a(1,z)}{A_a(1,2)}\right.\right.$$
$$\left.\left.\times\,\frac{(\theta_{\text{ion}} - \theta^*_{\text{ion}})\,\theta_a}{(\theta^*_{\text{ion}} - 3\theta_a)\,[(\theta^* + 2\theta_a)\exp(\theta^*_{\text{ion}}/\theta_a) + \frac{1}{2}(\theta_{\text{ion}} + 2\theta_a)]}\right] + \theta_{\text{ion}}\right\} s_{aa},$$

$$q_{ae} = \frac{4\sigma_R \pi^{\frac{1}{2}} m_e e^{\theta^*}}{A_e(1,2)\,k T_0 m_a}\,\bar{n}^2\,\frac{\theta_e^{\frac{1}{2}}(\theta_a - \theta_e)}{\theta^* + 2}\left[1 - 3\,\frac{\theta_R}{\theta_e} + \ldots\right],$$

$$q_{ie} = \frac{e^4 \pi m_e e^{\theta^*}}{A_e(1,2)\,(k T_0)^3 m_a}\,\bar{n}^2\,\frac{\theta_a - \theta_e}{\theta_e^{\frac{3}{2}}(\theta^* + 2)}\ln\Lambda,$$

where $$\bar{A}_a(1,2) = \frac{A_a(1,2)}{A_e(1,2)}, \quad \bar{n} = \frac{n_a + n_i}{n_{a0}}$$

and $\bar{x}$ is a non-dimensional distance defined by the expression

$$\bar{x} = \frac{x}{u_0 n_{a0}[R_e(1,2)]_{T_e = T_0}},$$

where the denominator is the relaxation distance of electron–atom collisions for an electron temperature equal to the initial atomic temperature. This non-dimensional distance was very convenient for computations since it does not

depend strongly upon the initial conditions and therefore the step size of integration established for one initial condition can be used for any other.

In the calculations we assumed that the ratio of $A_a(1,z)/A_a(1,2)$ is unity. Since this ratio is multiplied by $\exp(-\theta^*_{\text{ion}}/\theta_a)$ the second term in the square brackets in the expression for s_{aa} is smaller than the first one and the above assumption is not important. Solution of the system for one particular shock speed and initial pressure is shown in figure 7. It indicates that the electron temperature practically coincides with the atom temperature everywhere except for a very small region near $x = 0$. This result is quite different from a similar

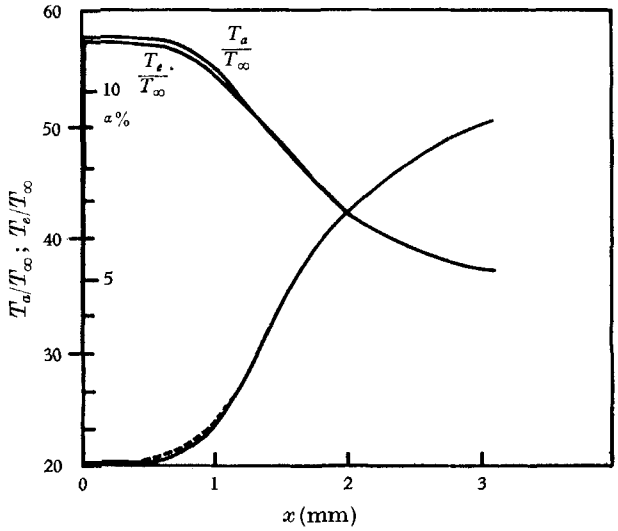

FIGURE 7. Temperature and degree of ionization profiles behind the shock front in hydrogen ($P_\infty = 3$ torr, $M_s = 25$). ———, exact solution; – – –, approximation $T_a \equiv T_e$.

solution for argon where the electron temperature is substantially smaller than the atomic temperature for most of the relaxation region. As we mentioned earlier this disparity between hydrogen and argon can be explained by the higher rate of energy transfer to the electronic component from the hydrogen atoms in comparison with the energy transfer from argon atoms.

This convenient aspect of the hydrogen plasma allows us to make substantial simplification of the equations. With the assumption that $T_a = T_e$ everywhere in the relaxation region, the equation for the electron temperature becomes redundant and therefore can be omitted. The solutions of the remaining system can be done by a direct integration:

$$\bar{x} = \int_0^\alpha \frac{d\alpha}{s_{aa}(1-\alpha)^2 + s_{ae}\alpha(1-\alpha) - s_{eei}\alpha^3},$$

$$\theta_a = \frac{\bar{n} + (\bar{n}-1)\,c}{\bar{n}^2(1+\alpha)},$$

$$\bar{n} = \frac{1 + c^2 + \{\frac{9}{25}c - (\frac{6}{5} - \frac{3}{25}\frac{2}{5}\alpha\theta_{\text{ion}})\,c\}^{\frac{1}{2}}}{2 - \frac{4}{5}\alpha\theta_{\text{ion}} + \frac{2}{5}c}, \tag{1.33}$$

where in the expression for s the electronic temperature should be set equal to the atomic temperature. Comparison of the solution of the system of equations (1.33) with the exact solution shows (see figure 7) that they practically coincide. This finding made the analysis of the experimental data much simpler.

2. Apparatus and experimental technique

Theoretical estimations showed that in hydrogen shock speeds greater than 2·5 cm/μsec ($M_s > 20$) are required if complete dissociation and a measurable electron concentration is to be obtained behind the shock. The conventional

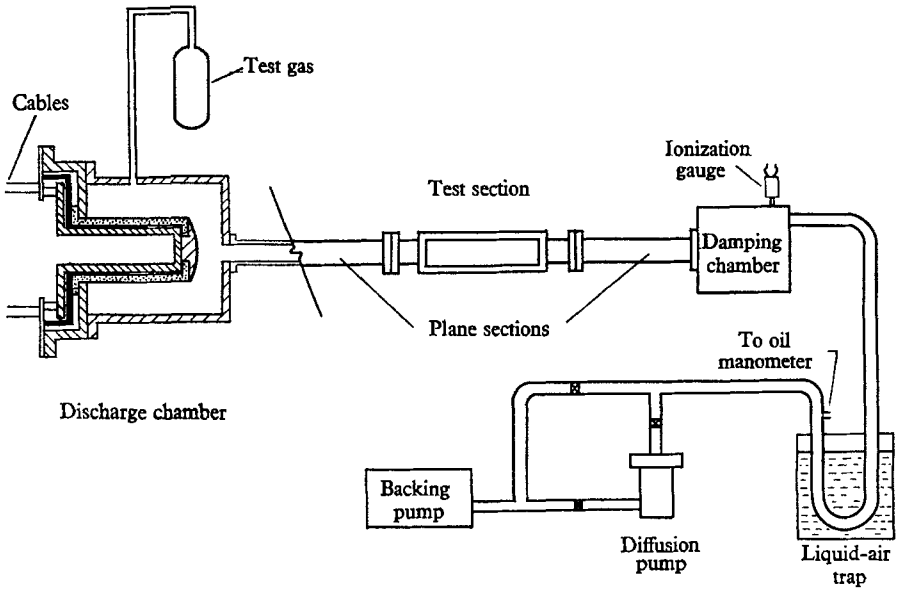

FIGURE 8. Electromagnetic shock tube facility.

diaphragm shock tube even with many improvements is still unable to produce shock wave velocities greater than 0·6 to 0·8 cm/μsec in air or argon and even less in hydrogen and helium (see Chang 1965). On the other hand, the recent advances in fast discharges in gases showed the possibilities of obtaining plasma velocities up to 100 cm/μsec (Dubovol & Nesterichin 1964).

Shock tube facility

A schematic diagram of the facility is shown in figure 8. The discharge chamber consists of a stainless-steel inner electrode (8 in. × 7 in. diameter) insulated from the outer stainless-steel chamber (9 in. × 12 in. diameter) by the cylindrical ceramic insulator. The energy stored in the capacitor bank is supplied to the inner electrode through 49 coaxial cables. The outer chamber has two apertures: one $\frac{1}{8}$ in. diameter for a test gas inlet (on the side wall) and a second, on the axis of the chamber, 1·5 in. diameter where the shock tube is connected to it. The shock tube itself is a square cross-section ($1\frac{1}{4}$ in. × $1\frac{1}{4}$ in.) stainless-steel tube made in three interchangeable sections each about 20 in. long, in order to observe the

shock behaviour at different distances from the discharge chamber. The test section has two 10 in. × 2 in. × $\frac{3}{8}$ in. observation windows. A capacitor bank, comprising seven sets of three 8·5 μF, 20 kV capacitors in parallel, energizes the discharge chamber. The details of this facility, its advantages and performance are described in detail by Belozerov (1968).

The planarity of the shock front was studied by the schlieren technique using the Q-spoiled pulse of a ruby laser ($\simeq$ 20 nsec duration) as a light source.

The two schlieren pictures shown in figure 9, plate 1, illustrate the extreme types of structure obtained. The first shows the turbulent driver plasma found close to the discharge chamber and corresponds to a high shock Mach number. The second indicates that at large distances from the discharge chamber a plane shock is formed with good separation between the shock front and the driver. At a distance of about 60 cm from the discharge chamber this separation was sufficient to study the relaxation processes.

Double-frequency interferometer

The Q-spoiled ruby laser has also proved to be a very effective light source for the Mach–Zehnder interferometer. The coherence and small beam divergence of this light source permit interference over long optical paths and allow considerable relaxation in the quality and precision of adjustment of the optical components of the interferometer. The spectral purity of the radiation makes it feasible to use narrow band pass filters to block unwanted radiation from the highly luminous phenomena such as the high-temperature plasma behind the shock, while the small beam divergence allows the use of a very small stop at the focus of the fringe-forming lens as an additional means of discriminating against such radiation. Furthermore, the Q-spoiled ruby laser readily provides a time resolution of the order of 20 nsec or less for the study of transient events.

Alpher & White (1959) first pointed out that it is highly desirable in the interferometric study of a plasma to make simultaneous measurements at two wavelengths. Since the refractivity of the free electrons is highly frequency dependent compared with the almost constant refractivity of the neutrals, the electron and neutral number densities can be readily obtained from two interferograms. An obvious extension to the use of the ruby laser is to make simultaneous measurement at both the fundamental laser wavelengths 6943 Å and its second harmonic of 3472 Å, generated by passing the beam through a non-linear optical medium. This technique was successfully used by Alcock & Ramsden (1966) to determine the electron density in a laser-induced spark in air.

Figure 10 shows the schematic diagram of the interferometer. The beam from the rotating-prism Q-spoiled ruby laser† with an output of 1 joule passes through a K.D.P. crystal and generates a collinear beam of second harmonic radiation at 3472 Å. The K.D.P. crystal was aligned with respect to the front mirror of the laser by an autocollimator and enclosed in a special box with two windows, where the humidity was kept at a low level by a heater in order to prevent damage

† TRG-104 laser with a cryptocyanine cell as a means of suppressing all the secondary pulses was used.

to the crystal. Simultaneous interferograms at 6943 Å and 3472 Å were taken by splitting the exit beam at the glass plate and using the narrow band interference filters, centred at the fundamental and the second harmonic of the laser radiation, one for each of the output beams. The second-harmonic filter was placed in the transmitted beam so that both interferograms were obtained with approximately the same intensity on the Polaroid Type 47 film. The radiation from the plasma

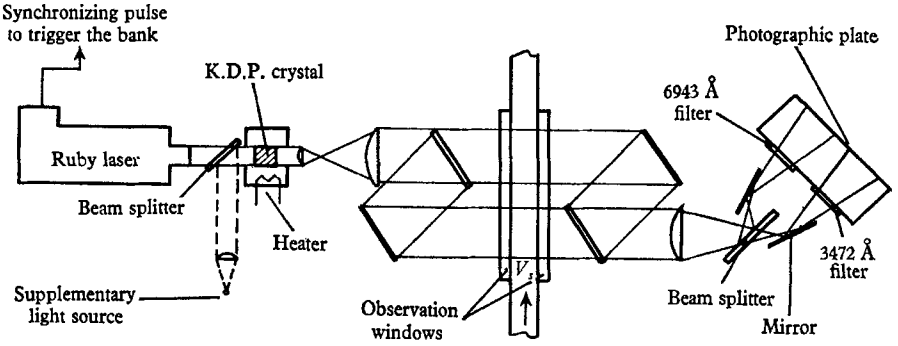

FIGURE 10. Schematic of double-frequency interferometer.

and the reflexion from the inner surface of the splitter were eliminated by two stoppers placed at the focal points of the beams.

The aperture of the interferometer was 3 cm × 5 cm. The region of the observation window nearest the discharge chamber was used for the test section and the other end of it was used as the compensation chamber. The interferometer was mounted on two half-inflated inner tubes in order to isolate it from the vibrations of the floor. The alignment of the interferometer was made before each run with a supplementary diffused light source to ensure the best contrast and horizontal position of fringes. The velocity of the shock wave in the observation section was measured with a photomultiplier arrangement with an estimated error of $< 0{\cdot}5\,\%$.† In order to know the position of the shock front at the moment of observation the laser pulse was registered by a separate photodiode arrangement.

Experimental procedure

Prior to each set of experiments the system was kept under continuous pumping at a pressure of 10^{-5} torr for several days. After this period of time the rate of leaks and outgassing was less than 10^{-5} torr/min. The time interval between runs of each series was not less than 2 h, during which the system was also kept under continuous pumping. Just before each run the system was flushed with the test gas (ultra-pure hydrogen with the specified impurity level 5 parts per million) for 2–3 min and then filled to the required pressure. Immediately after this the bank was charged and fired within approximately a 1 min interval.

When the refractive index N of the gas in one arm of the interferometer is changed by an amount ΔN, the corresponding change in the optical path $l\Delta N$ produces a phase shift S for radiation of wavelength λ:

$$S = l\Delta N/\lambda; \tag{2.1}$$

† The oscilloscope time base was calibrated by a special time delay unit to within an accuracy of 0·1 %.

l is the length of the gas for which the refractive index changes by ΔN. The change in the refractive index, $\Delta N = N - N_0$, is the result of the density jump and the appearance of free electrons, N_0 is the refractive index ahead of the shock and N is the index in some plane of interest behind the shock.

The general expression for the refractive index of a gas consisting of several species can be written in the form

$$N = 1 + 2\pi \sum_i \xi_i n_i - \tfrac{1}{2}(\omega_p/\omega)^2. \tag{2.2}$$

Here, n_i is the number density of the species i with a polarizability ξ_i. The last term is the contribution from the free electrons where ω is the impressed frequency and the plasma frequency ω_p is given by the expression

$$\omega_p = (4\pi n_e e^2/m_e)^{\frac{1}{2}}.$$

The ion contribution to the refractive index is a factor m_e/m_a smaller than the electron contribution and is therefore omitted in the above expression.

The relevant values for the refractive index of molecular hydrogen are determined from the work of Landolt & Börnstein (1962):

$$N^0_{H_2} = 1 + 1.384 \times 10^{-4} \quad \text{for} \quad \lambda = \lambda_1 = 6943\,\text{Å},$$
$$N^0_{H_2} = 1 + 1{\cdot}453 \times 10^{-4} \quad \text{for} \quad \lambda = \lambda_2 = 3472\,\text{Å}.$$

Using the Gladstone–Dale relation, $N^0_{H_2} - 1 = 2\pi\xi_{H_2} n_L$ where the Loschmidt number $n_L = 2{\cdot}687 \times 10^{19}\,\text{cm}^{-3}$, we obtain the polarizabilities for molecular hydrogen

$$\left.\begin{aligned}(\xi_{H_2})_{\lambda=\lambda_1} &= 5{\cdot}52 a_0^3,\\ (\xi_{H_2})_{\lambda=\lambda_2} &= 5{\cdot}81 a_0^3.\end{aligned}\right\} \tag{2.3}$$

The polarizability of atomic hydrogen was studied theoretically and experimentally by Marlow & Bershader (1963). They obtained very good agreement between experimental and theoretical values of ξ_H for the wavelength of 5870 Å.

The contribution (to the refractive index) from excited atoms is negligible (see Korobeynikov, Melnikova & Ryozanov 1961) in the visible region of the spectrum; consequently the refractive index behind the shock front with complete dissociation will only be determined by the atomic and electron refractivities. However, the refractive index of the gas ahead of the shock is completely determined by (2.3); therefore a fringe shift ΔS can be written in the following final form:

$$\left.\begin{aligned}\Delta S_{\lambda_1} &= 1{\cdot}82 \times 10^{-7} \frac{l p_\infty}{\lambda_1}\left(1{\cdot}67 \frac{n_a}{n_\infty} - 1\right) - 4{\cdot}49 \times 10^{-14} \lambda_1 l n_e,\\ \Delta S_{\lambda_2} &= 1{\cdot}91 \times 10^{-7} \frac{l p_\infty}{\lambda_2}\left(1{\cdot}71 \frac{n_a}{n_\infty} - 1\right) - 4{\cdot}49 \times 10^{-14} \lambda_2 l n_e,\end{aligned}\right\} \tag{2.4}$$

where the dimensions of l and λ_1 are cm and p_∞ is measured in torr.

The electron number density and number density of neutral atoms can be expressed from (2.4) in terms of the experimentally obtained fringe shifts ΔS_{λ_1} and ΔS_{λ_2} in the form

$$\left.\begin{aligned}n_e &= (1{\cdot}94 \times 10^{17}/l)\,[2{\cdot}15 \Delta S_{\lambda_1} - \Delta S_{\lambda_2}) + 1{\cdot}3 \times 10^{-4} p_\infty l],\\ n_a/n_\infty &= (68{\cdot}9/l p_\infty)\,(\Delta S_{\lambda_1} - 2\Delta S_{\lambda_2}) + 0{\cdot}578.\end{aligned}\right\} \tag{2.5}$$

The last term in the first expression can be omitted because it is much smaller than the experimental error in ΔS. In the present test section $l = 2{\cdot}85$ cm.

3. Experimental results and discussion

General description of interferograms

A number of preliminary runs indicated that for optimum operational conditions the range of the initial pressure should be from 1·5 torr to 3 torr and that the observation distance should be 65 cm from the discharge chamber. Variation of the capacitor bank voltage between 14 and 17 kV generated velocities in the range from 2·8 cm/μsec ($M_s \simeq 21$) to 3·5 cm/μsec ($M_s \simeq 26$).

A typical two-frequency interferogram is shown in figure 11 (*a*), plate 2. The manner in which the fringes are shifted shows changes of the refractive index of the gas determined by several relaxation processes behind the shock. In the shock front the fringes were shifted owing to the density jump associated with the translational shock and dissociation. The density of the flow right after this sudden deflexion of the fringes agreed well with the theoretically predicted values obtained from the relations (1.30) for a dissociative shock. The zero-order interferogram corresponding to the same flow condition is shown in figure 11 (*b*), plate 2.

After a sufficient number of electrons were produced the fringes start to shift in the opposite direction to the initial jump, with the fringe shift for the first harmonic appreciably larger than for the second one. The axial distance between the first fringe shift and the second one depended on the velocity of the shock and the initial pressure. This relaxation distance was of the order of a mm or so for the velocities of interest. The length of the equilibrium region which exists behind the second prominent fringe shift varied also from run to run and was of the order of several mm on the average. The contact surface which follows the equilibrium region appears as a further steep increase in the electron number density. In contrast with the ionization front the contact surface is not a plane surface but usually is an asymmetrically curved region, which qualitatively correlates with the schlieren pictures discussed earlier. In some of the runs which were considered 'bad' and were not used in the calculations the driver plasma from behind the contact surface penetrated the whole relaxation region. In figures 11 (*c*) and (*d*), plate 2, a comparison is shown which illustrates the difference between a perturbed and unperturbed shock front, respectively.

Analysis of the experimental errors

There are several sources of errors which could influence the accuracy of the determination of the desired atom–atom cross-section. The photomultiplier arrangement enables the velocity of the luminosity front to be measured with an accuracy of about $\pm 0{\cdot}5\,\%$. If the shock velocity is high enough to produce a sufficient number of electrons behind the shock the velocity of the luminosity front would be the same as for the shock front. For lower speeds (we found this limit to be about 2·5 cm/μsec) ionization of the shock wave is negligible and the photomultiplier would record the motion of the driver plasma at a speed which is not necessarily equal to the speed of the shock front.

Measurements of the fringe shifts are accurate within $\frac{1}{10}$ of a fringe, which gives an uncertainty in the electron number density of about $\pm 10^{16}\,\mathrm{cm}^{-3}$ and an uncertainty in the neutral density jump n/n_∞ of $\pm p^*/p_\infty$, where p^* is equal to 2 torr.

According to our theoretical assumptions the origin of the relaxation distance for ionization coincides with the point behind the shock front where dissociation is completed. However, in practice, it is impossible to define this point accurately

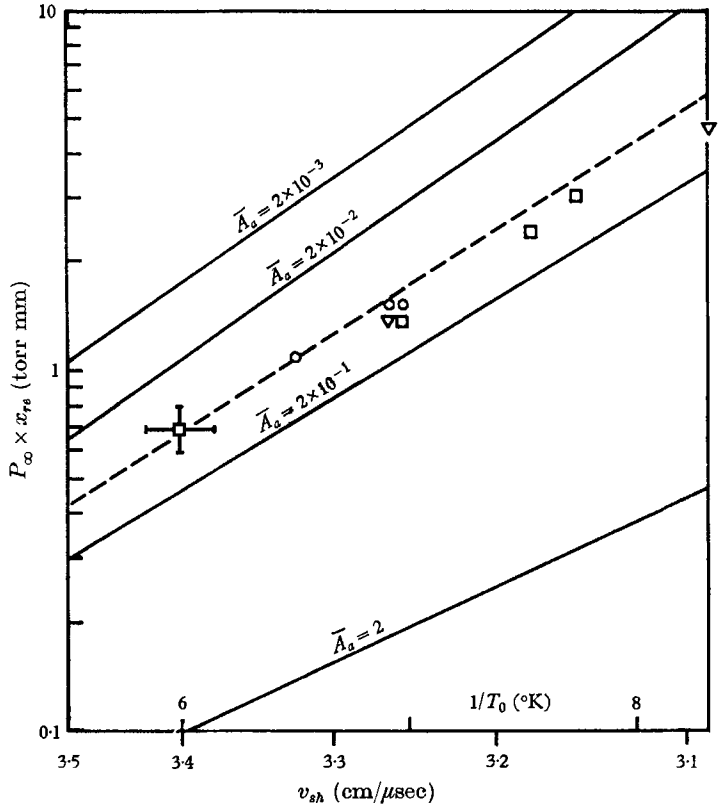

FIGURE 12. Comparison of experimental initial relaxation length with theoretical length calculated for different atom–atom cross-section. Initial pressure: ▽, 3 torr; ○, 2 torr; □, 1·5 torr.

so instead the point where the density rise reaches half of its peak value corresponding to the complete dissociation was taken as the origin. This procedure would compensate partially for an error which is introduced in the theory by the assumption that no electrons are produced in the region of dissociational relaxation. The estimated absolute error in the evaluation of the distance from the interferograms was $\pm 0{\cdot}1$ mm, the relative error was not more than $\pm 0{\cdot}02$ mm. The initial pressure was set by means of an oil manometer with an accuracy of about $\pm 0{\cdot}01$ torr. The combined uncertainty in the relaxation distance and the shock speed prevents the cross-section from being determined with an accuracy better than about an order of magnitude. We consider this to be sufficient at the

present time because no theoretical or other experimental results on this cross-section are available.

Comparison of experimental results with the theory

The experimental initial relaxation distance has been defined as the distance from the middle of the dissociative front to the point where the electron number density equals $\frac{1}{10}$ of its equilibrium value. This distance is plotted on figure 12 together with the theoretical values for different atom–atom cross-sections. The

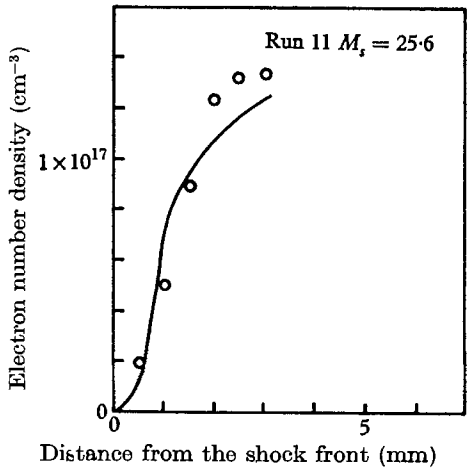

FIGURE 13. Comparison between theoretical (curve) and experimental (circles) electron density profiles.

experimental points appear to lie on a theoretical curve corresponding to the value of $\bar{A}_a = 7\times10^{-2}$. Comparison of the theoretical and experimental electron density profiles, figure 13, indicates the good agreement.

4. Concluding remarks

The present theoretical and experimental studies of the relaxation processes behind a strong shock wave produced in hydrogen in an electromagnetic shock tube enable us to state the following conclusions: (i) the calculated electron and atomic temperatures in the ionizational relaxation region behind the shock front in hydrogen become practically equal to each other in a very small distance (of the order of 0·1 mm) and therefore the differential equation for the balance of electron energy is redundant in the system of equations describing the relaxation processes in the shock; (ii) with the assumption at equipartition of energy between the three particles resulting from an atom–atom ionizing collision the initial temperature for the electrons can be calculated theoretically. It is found to be equal to $\frac{4}{9}$ of the initial atomic temperature (defined as the temperature behind the dissociative shock) for the case when $kT \ll E_{\text{ion}}$. Although this result is not important for shocks in hydrogen because of what has been stated in the first conclusion it might be used in the calculations of the electron temperature profiles

in heavy gases where substantial difference between atomic and electron temperature is expected; (iii) for the range of shock velocities of interest and for an initial pressure of 1 torr and above, the collisional processes dominate the radiative ones in the ionizational relaxation region and therefore the latter can be ignored; (iv) the electromagnetic shock tube with a Philippov pinch as the driver is able to produce plane shocks with a speed varying from 2 to 5 cm/μsec at distances from 60 to 80 cm from the discharge chamber in hydrogen at an initial pressure in the range from 0·1 to 10 torr; (v) the double-frequency interferometer with a ruby Q-spoiled laser coupled with a K.D.P. crystal as a light source enables interferograms at two wavelengths, 6943 Å and 3472 Å, to be obtained of highly luminous, high-speed events with the effective exposure time of the order of 10 nsec; (vi) the mean slope of the cross-section curve for atom–atom excitation collisions (from the ground state to the first excited state) calculated from the comparison of the theoretical and experimental relaxation lengths is $7 \times 10^{-2} A_e(1,2)$ (with an uncertainty in the result being a factor of 5), where $A_e(1,2)$ is the corresponding known mean slope of the cross-section curve for electron–atom collisions.

The authors are grateful to Dr G. N. Patterson, Director of the Institute for Aerospace Studies, for his interest in the reported research and one of us, A.N.B., would like to thank Dr Patterson for the opportunity of studying at UTIAS. The authors would also like to express their special gratitude to Dr J. H. de Leeuw for many stimulating discussions and valuable suggestions and to Mr A. Jaskolka for his assistance with the computer programming.

This research was supported by the Defence Research Board of Canada (Grant No. 9551-02) and by the United States Air Force Office of Scientific Research under AFOSR Grant No. 366-66.

Appendix. Simplification of the rate equations for ionization in atom–atom collisions

The rate of ionization and excitation into the first excited state can be described consequently by the equation

$$dn_e/dt = \tfrac{1}{2} R_a(1,z)\, n_a^2 + R_a(2,z)\, n_a n^*, \tag{A 1}$$

$$dn^*/dt = \tfrac{1}{2} R_a(1,2)\, n_a^2 - R_a(2,z)\, n_a n^* - R_a(2,1)\, n_a n^*, \tag{A 2}$$

where $R_a(1,z)$, $R_a(1,2)$ are the rate coefficients for ionization and excitation from the ground state, $R_a(2,z)$ is the rate coefficient for ionization from the excited state. In the above expression we neglected all the processes including the higher excited states and assume that radiative decay of the first excited level is not important because the mean free path of this radiation is very small (10^{-4} cm) so that the resonance radiation is trapped in the gas. If we assume that n_a is constant, the solution of (A 2) with $n^* = 0$ at $t = 0$ is

$$n^* = \frac{1}{2} \frac{R_a(1,2)\, n_a}{R_a(2,z) + R_a(2,1)} \{1 - \exp(-[R_a(2,z) + R_a(2,1)]\, n_a t)\}. \tag{A 3}$$

For any time $$t^* \gg \frac{1}{[R_a(2,z)+R_a(2,1)]n_a},$$

there will be a simple direct relation between n^* and n_a,

$$n^* \simeq \frac{1}{2}\frac{R_a(1,2)}{R_a(2,z)+R_a(2,1)}n_a. \tag{A 4}$$

Time t^* is estimated to be an order of $10^{-2}\,\mu$sec, which is negligible for most practical purposes.

Substituting (A 4) into (A 1) we have

$$\frac{dn_e}{dt} = \frac{1}{2}\left[R_a(1,z)+R_a(1,2)\frac{R_a(2,z)}{R_a(2,z)+R_a(2,1)}\right]n_a^2, \tag{A 5}$$

where the fraction in the last term, being an order of unity, was neglected in the calculations.

REFERENCES

Ahlstrom, H. G., Mahaffey, D. W., Sanga, L. & Schoen, R. I. 1963 Boeing Report, ND 1-82-0321.

Alcock, A. J. & Ramsden, S. A. 1966 *Appl. Phys. Lett.* **8**, 187.

Alpher, R. A. & White, D. R. 1959 *Phys. Fluids*, **2**, 162.

Appleton, J. P. 1966 *Phys. Fluids*, **9**, 336.

Bates, D. R., Kingston, A. E. & McWhirter, R. W. P. 1962 *Proc. Roy. Soc.* A **270**, 155.

Belozerov, A. N. 1968 *UTIAS* Rep. no. 131.

Bond, J. W. 1957 *Phys. Rev.* **105**, 1682.

Brackmann, R. T., Fite, W. L. & Naynamber, R. M. H. 1958 *Phys. Rev.* **112**, 115.

Burgess, A. 1963 *Proc. 3rd Int. Cong. Physics of Electronics and Atomic Collisions.*

Chang, C. T. 1962*a* *RISO* Rep. no. 35.

Chang, C. T. 1962*b* *RISO* Rep. no. 46.

Chang, C. T. 1965 *Proc. 7th Int. Cong. Phenomena in Ionized Gases.*

Cloupeau, M. 1963 *Phys. Fluids*, **6**, 679.

deBoer, P. C. T. 1967 *Phys. Fluids*, **10**, 2485.

Dubovol, A. V. & Nesterichin, Y. E. 1964 *Dokl. A. N. USSR* **154**, 1310.

Fite, W. L. & Brackmann, R. T. 1958 *Phys. Rev.* **112**, 1191.

Glass, I. I. & Hall, J. G. 1959 *Handbook of Supersonic Aerodynamics Section* 18, *Shock Tubes*, NAVORD Rep. 1488, Vol. 6.

Gryzinski, M. 1959 *Phys. Rev.* **115**, 374.

Harwell, K. E. & Jahn, R. G. 1964 *Phys. Fluids*, **7**, 214.

Korobeynikov, V. P., Melnikova, N. S. & Ryozanov, Y. V. 1961 *Teoriya Tochechnogo Vzryva, Moscow.*

Landolt, H. & Börnstein, R. 1962 *Zahlenwerte und Funktionen*, vol. 2, no. 2*b*. Berlin: Springer-Verlag.

Lichten, W. & Schultz, S. 1959 *Phys. Rev.* **116**, 1132.

Marlow, W. C. & Bershader, D. 1963 Dept. Aeron. Astron., Stanford University. SUDDAR no. 149.

McLean, E. A., Faneutt, E., Kole, A. C. & Griem, H. R. 1960 *Phys. Fluids*, **3**, 843.

Oettinger, P. E. 1966 Dept. Aeron. Astron., Stanford University. SUDDAR, 285.

Petschek, H. & Byron, S. 1957 *Ann. Phys.* **1**, 270.

Philippov, N. V. & Philippova, T. I. 1965 Report I.A.E. 913, I.V. Kurchatov Institute Moscow.

Philippov, N. V., Philippova, T. I. & Vinogradov, V. P. 1962 *Nucl. Fusion Suppl.* Pt. 2, p. 577.

PRESNYAKOV, L., SOBELMAN, I. & VAISHTEIN, L. 1963 *Proc. 3rd Int. Cong. Physics of Electronic and Atomic Collisions.*

STABBINGS, R. F., FITE, W. L. HUMMER, D. G. & BRACKMAN, R. T. 1960 *Phys. Rev.* **119**, 1939.

TEMKIN, A. & LAMKIN, J. C. 1961 *Phys. Rev.* **121**, 788.

WETZEL, L. 1964 *AIAA J.* **2**, 1208.

WEYMANN, D. H. 1958 Inst. Fluid Dyn. Appl. Math. University of Maryland. TN no. BN-144.

WIESE, W., BERG, H. F. & GRIEM, H. R. 1960 *Phys. Rev.* **120**, 1079.

WONG, H. & BERSHADER, D. 1966 *J. Fluid Mech.* **26**, 459.

ZHURIN, V. V. & SULYEAV, V. A. 1963 *Engng J. III*, **4**, 645.

ZHURIN, V. V., SULYEAV, V. A. & BUKOVSKII, V. M. 1963 *Engng J. III*, **4**.

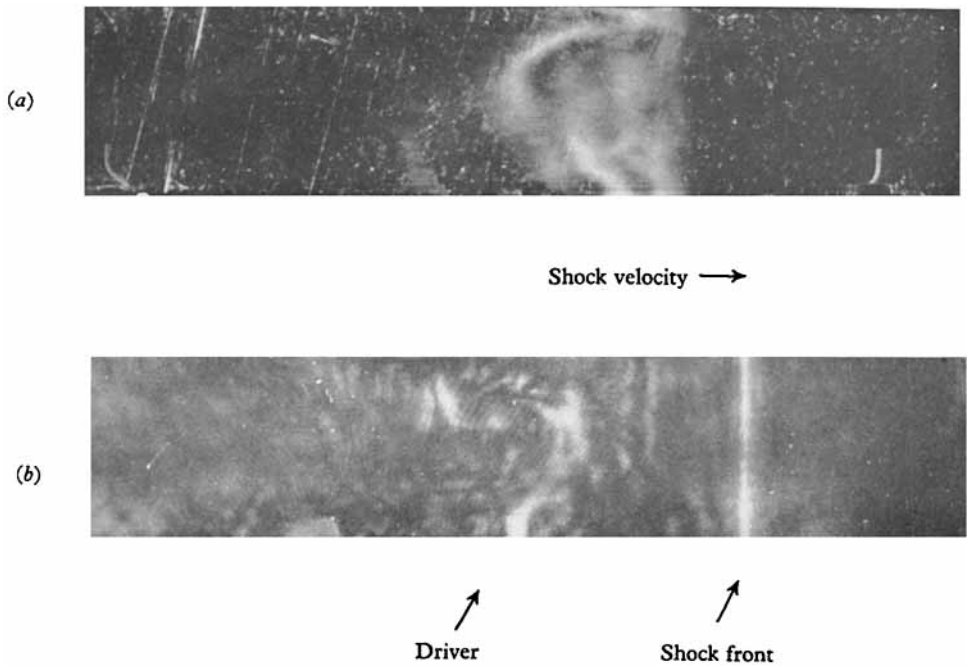

FIGURE 9. Schlieren pictures of the shock wave formation: (*a*) $M_{sh} = 70$, $P_\infty = 1$ torr, distance from the discharge chamber, 35 cm. (*b*) $M_{sh} = 30$, $P_\infty = 1$ torr, distance from the discharge chamber, 60 cm.

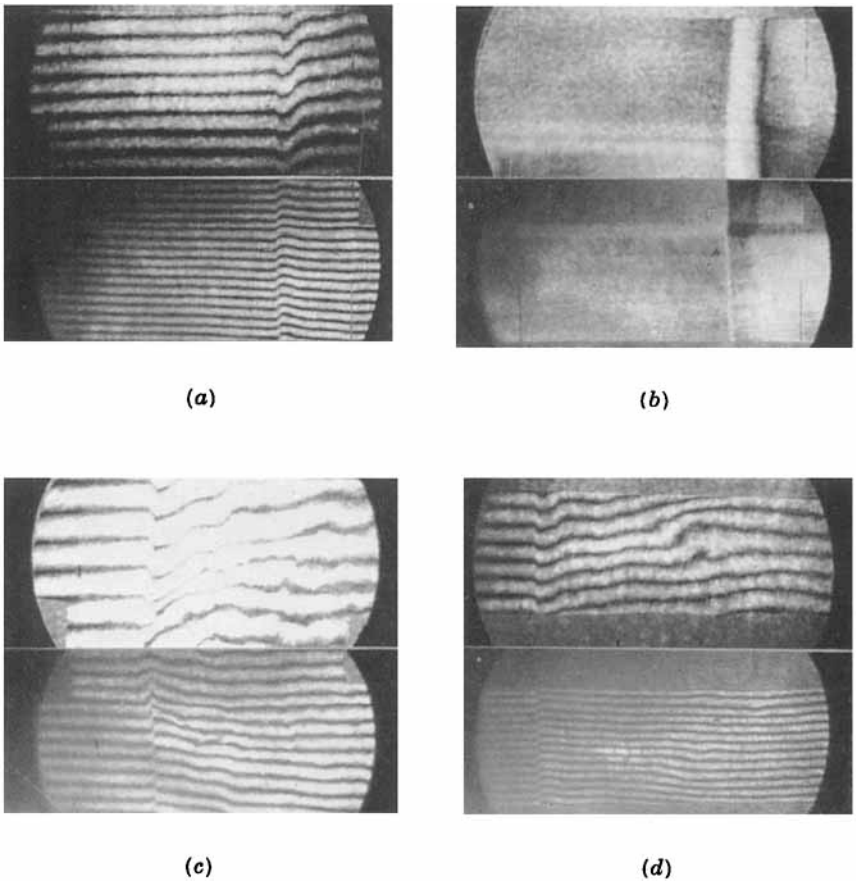

FIGURE 11. Typical interferograms. (*a*) $M_{sh} = 23{\cdot}4$, $P_\infty = 3$ torr. (*b*) $M_{sh} = 23{\cdot}4$, $P_\infty = 3$ torr, zero-order interferogram. (*c*) Strong interaction of the driver gas with the shock. (*d*) No interaction.